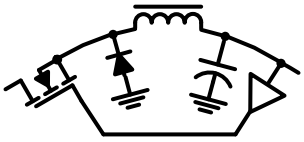

Power Supply Design Seminar

Dual Active Bridge Topology Overview

Texas Instruments

Reproduced from
2026 Texas Instruments Power Supply Design Seminar
SEM2600
Topic 3
Guangzhi Cui and Will Tai
Literature Number: SLUP430

Power Supply Design Seminar resources
are available at:
www.ti.com/psds

The Dual Active Bridge (DAB) converter is a popular topology in high-performance bidirectional DC-DC converters when fast transient response, wide input/output range and high efficiency are required. This paper introduces the characteristics of the DAB converter, single-phase shift DAB converter operation principles, multiple freedoms optimization process in DAB converter design, series resonant DAB (SR-DAB) converter features and its control methods. A SR-DAB converter design based on the Energy Storage Systems (ESS) applications demonstrates the performance of a SR-DAB converter, which supports wide input/output range and has a high efficiency in full load range.

Introduction

With the growing development of sustainable energy and electric end-equipment(1), the large-scale application of bidirectional DC-DC converters continues to grow. Bidirectional DC-DC converters serve widely as power interface in wind power generation, photovoltaic power generation, Electrical Vehicles chargers, and ESS as shown in **Figure 1**. Among these applications, this discussion takes ESS as a target application to explain why DAB converter gains popularity in such applications.

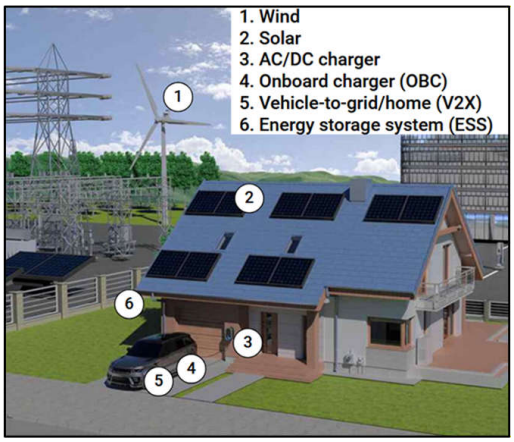

Figure 1. *Sustainable ecosystem model.*

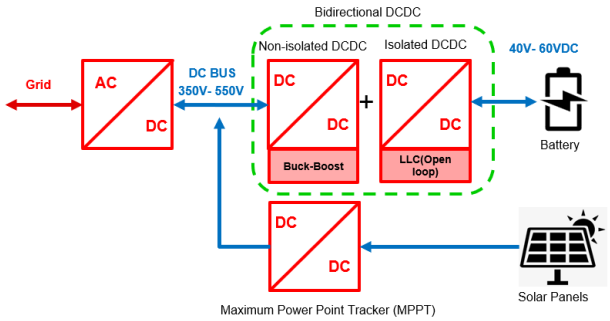

Figure 2. *Block diagram of two stage residential ESS.*

Figure 2 shows a typical residential ESS system, where a high-voltage DC bus interfaces the electric grid and the battery system. The energy generated by the solar panels is converted by a unidirectional DC-DC converter and fed to the bus, typically referred to as Maximum Power Point Tracker (MPPT), then connects to the bus. This energy transfers to the electric grid by an inverter or stores in the battery system. Here, a bidirectional DC-DC converter charges or discharges the battery. Low voltage batteries (for example, 48V) find wide use in residential ESS because of safety considerations. Therefore, isolated DC-DC converters must provide galvanic isolation between the high-voltage DC bus and the battery.

As **Figure 2** shows, a traditional bidirectional DC-DC converter comprises two stages: a buck-boost converter and an inductor-inductor-capacitor (LLC) converter. The LLC converter achieves isolation and operates at the converter resonant point (open loop operation) to achieve high efficiency. The closed loop buck-boost converter adjusts the gain voltage and meets system dynamic response. A two-stage approach usually has lower power density and higher cost even though the approach remains easy to design and control.

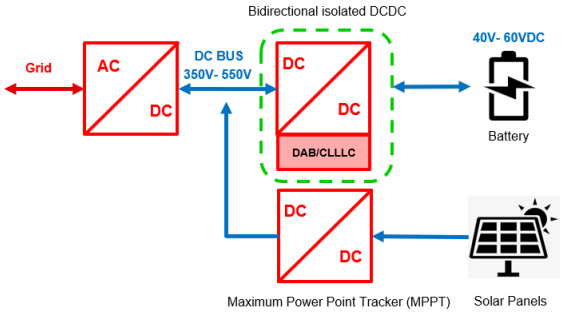

Figure 3. *Block diagram of one stage residential ESS.*

To optimize the performance and cost of this bidirectional isolated block more products implement a one stage approach as **Figure 3** shows. Four isolated DC-DC converter topologies, LLC series resonant converter (LLC)[2], CLLLC series resonant converter (CLLLC)[3], dual active bridge converter (DAB)[3], and series resonant dual active bridge converter (SR-DAB)[4], find wide application in battery charger applications today or attract interest because of advantageous characteristics in certain applications. Key characteristics of these four topologies are summarized in **Table 1**. Among these single stage topologies, converters like LLC and CLLLC achieve the full operating range zero voltage switching, while having low turn-off current in rectifier side. However, when the converter operates in wide input output ratio range scenario, the converter needs to trade off efficiency and wide gain range, which makes efficiency drop significantly. Besides, LLC and CLLLC converters use frequency modulation for voltage regulation and have slower response to load transient. Considering the above challenges, a DAB or SR-DAB converter represents a preferred choice in applications that need to cover wide input or output ranges without having much efficiency reduction and transient response degradation. This DC-DC converter requires a more complex control scheme to maintain performance in all the operating points. More comparison details between different topologies appear in [5]. In this topic, the discussion describes the fundamentals of a DAB converter including operational principles, multiple freedoms optimization process and SR-DAB converter overview, along with a SR-DAB converter design example.

LLC	CLLLC	DAB	SR DAB
Benefits: • Low turn-off current in rectifier side • Full range ZVS • High efficiency especially when operating at resonant frequency	**Benefits:** • Low turn-off current in rectifier side • Full range ZVS • Symmetric gain features • High efficiency especially when operating at resonant frequency	**Benefits:** • Wide voltage adjust range • Low cost • Fast dynamic response • High efficiency when voltage ratio matches transformer ratio	**Benefits:** • Wide voltage adjust range • Lower turn off current compared to DAB • Wider ZVS range than DAB
Challenges: • Narrow gain range (trade off efficiency and wide gain range) • Gain below one in reverse mode • Complex Synchronous Rectification (SR) control strategy	**Challenges:** • Narrow gain range (trade off efficiency and wide gain range) • Complex Synchronous Rectification (SR) control strategy • Potential for more discrete components	**Challenges:** • Low efficiency and high turn off current with single phase control • Hard to realize ZVS at light load • Complex control method to optimize the performance	**Challenges:** • Low efficiency with single phase control • Complex control method to optimize the performance

Table 1. *Summary of different topologies.*

DAB Operation Principles and Control Methods Introduction

Single-Phase-Shift (SPS) DAB Operation Principles

Figure 4 shows the circuit topology of DAB converter. This topology consists of two full-bridge structures which are connected to the input (V_1) and output ports (V_2). The switching nodes of the two full-bridges are connected correspondingly to a series inductor (L_s) and to a high-frequency isolation transformer (T_1).

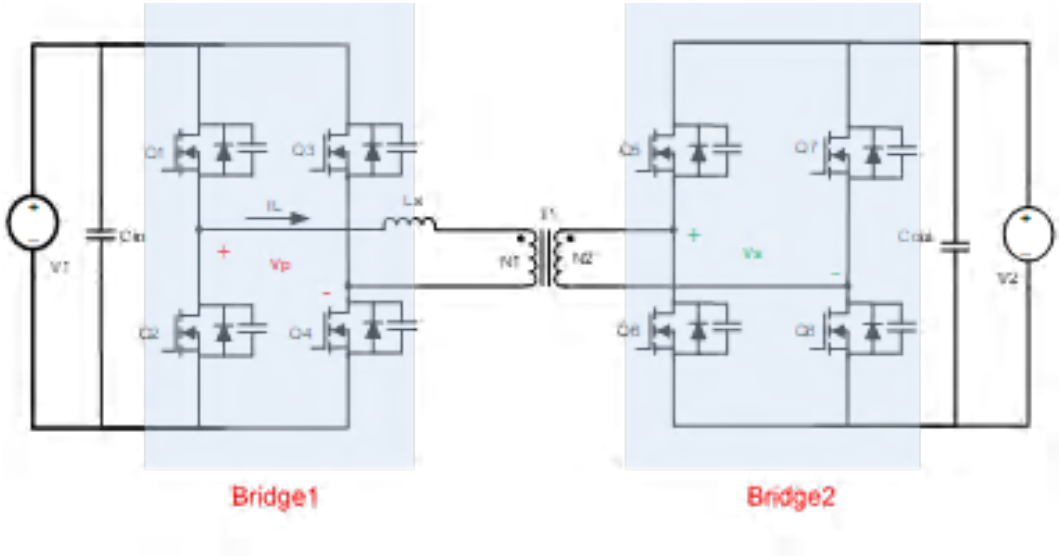

Figure 4. *Schematic of DAB converter.*

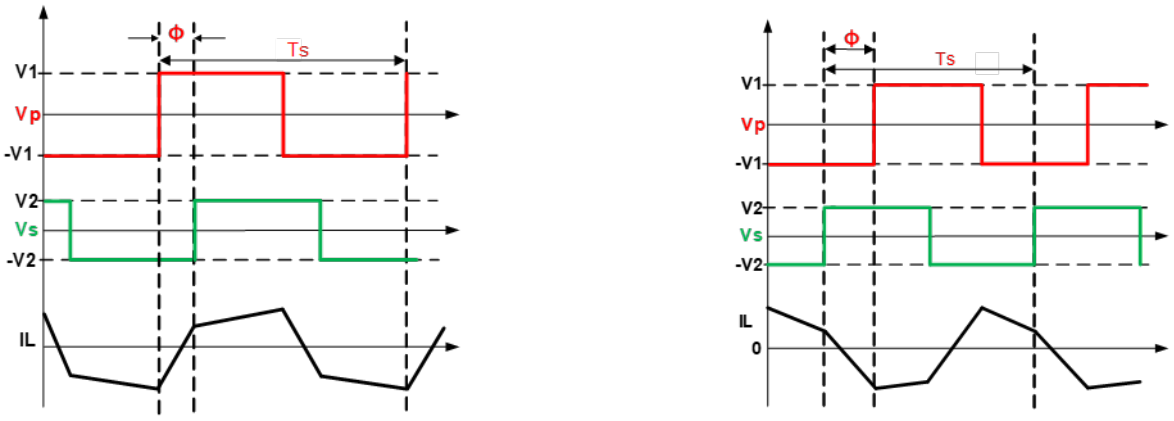

(a) Forward mode (0 ≤ Ø ≤ π).

(b) Reverse mode (–π ≤ Ø ≤ 0).

Figure 5. *DAB waveforms under SPS control*

Figure 5 shows the DAB converter waveforms under SPS control, the cross-connected switch pairs in both the full bridges are switched on to generate phase-shifted square waves with 50% duty ratio at the transformer's primary and secondary sides. The converter operates with a fixed switching frequency f_s, which is equal to $1/T_s$ (T_s is the switching period as shown in **Figure 5**). The FETs on the high side and low side of each leg are complementary conducting and the dead time between high-side and low-side FETs are necessary to avoid the shoot-through. By adjusting the phase shift angle Ø between Bridge 1 and Bridge 2, the direction and the amount of transmission power can be controlled. When the primary switch node voltage (Vp) leads the secondary side voltage (Vs), the power flows from the primary to the secondary (forward mode). When Vp is lagging the Vs, the power flows from the Bridge 2 to the Bridge 1 and the DAB is working in reverse mode. By assuming that all the components are ideal and by ignoring the dead time, the transition power can be calculated using **Equation 1**.

$$P_{12} = \frac{N \times V_1 \times V_2 \times \emptyset \times (\pi - \emptyset)}{2 \times \pi^2 \times L_s \times f_S} (-\pi \leq \emptyset \leq \pi) \quad (1)$$

where

- N is transformer turn ratio which is equal to N_1/N_2, N_1 is the primary winding turns and N_2 is secondary winding turns
- L_s is the inductance value of series inductor

The maximum transfer power is achieved when Ø is equal to π/2, thus achieving:

$$P_{max} = \frac{N \times V_1 \times V_2}{8 \times L_s \times f_S} \quad (2)$$

It is important to notice that the maximum transfer power is limited by the inductance value and the switching frequency.

To better understand the operation principle and the mode under SPS control of a DAB converter let's look at the waveforms in **Figure 6**. As depicted in the graph, switches Q1–Q4 form the primary side full bridge of a DAB converter and are modulated to generate V_p. The secondary side full bridge of the converter consists of Q5–Q8, which are modulated to generate a voltage V_s. To simplify the analysis process, we assume that the converter is operating in

steady-state. Based on the time sequence from t0 to t3 in **Figure 6**, the switching cycle can be divided into five operation modes in **Figure 7**, which are explained as follows:

1. Mode 1 (t0 to t0'): **Figure 7(a)** shows the equivalent circuit for the mode 1. Just before t0, Q2 and Q3 are conducting. The current IL is in negative direction and decreases linearly. Q2 and Q3 turned off at t0, and there will be high turn-off loss on Q2 and Q3, because the turn-off current is at the peak point. During t0 to t0', which is the dead time in the primary branch, the energy stored in the inductor discharges the output capacitors of Q1 to Q4 and charge the capacitors of Q2 and Q3. The inductor current is freewheeling through the body diode of Q1 and Q4 on the primary side. On the secondary side, the current is still flowing through Q6 and Q7.
2. Mode 2 (t0' to t1): **Figure 7(b)** shows the equivalent circuit for mode 2. The current IL is still in the negative direction during t0' to t1 and decreases to zero at t1. Q1 to Q4 turns on at t0' in the primary side and the voltage across Q1 and Q4 approximates to zero due to the conduction of their body diodes, which means the turn on is done in zero voltage switching (ZVS). On the secondary side, the current passes through the Q6 and Q7.
3. Mode 3 (t1 to t2): **Figure 7(c)** shows the equivalent circuit for mode 3. The current changes to positive direction after t1 and all switched status are the same as mode 2. This mode ends up when Q6 and Q7 are turned off. During mode 1 to mode 3, the inductor voltage is clamped at V1 + N × V2, the current of L_S is:

$$I_L(t) = I_L(t0) + \frac{N \times V_2 + V_1}{L_S} \times \left(t - t0\right) \tag{3}$$

4. Mode 4 (t2 to t2'): **Figure 7(d)** shows the equivalent circuit for mode 4. The time interval investigated is when dead time is applied on the secondary side. Q1 and Q4 is still on in primary side. On the secondary side, Q6 and Q7 are turned off at t2, there is turn-off loss on Q6 and Q7 because the turn-off current is not zero. During the dead time, the transformer current charges the output capacitors of Q6 and Q7, discharges the capacitors of Q5 and Q8, then the current is freewheeling through the body diode of Q5 and Q8.
5. Mode 5 (t2' to t3): **Figure 7(e)** shows the equivalent circuit for mode 5. At t2', Q5 and Q8 turns on, the current in the secondary side switches from the body diode to the channel of Q5 and Q8. The status in the primary side is the same as before. During mode 4 to mode 5, the inductor voltage is $V_1 - N \times V_2$, the current of L_s is:

$$I_L(t) = I_L(t2) + \frac{V_1 - N \times V_2}{L_S} \times \left(t - t2\right) \tag{4}$$

Similarly, the same principle can be applied to other FETs during t3 to t6. Therefore, the inductor current and voltage equation of each stage can be deduced which can be used to analyze this topology.

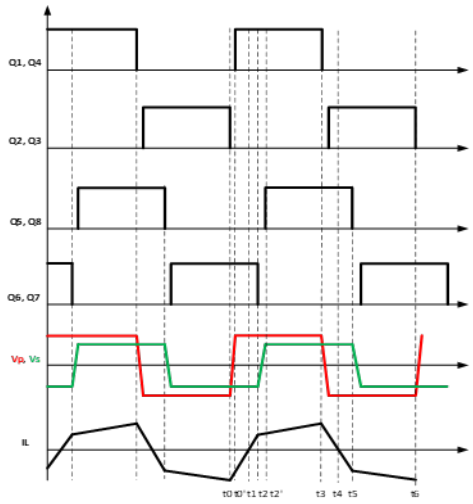

Figure 6. *DAB waveforms under SPS control with all switches driving.*

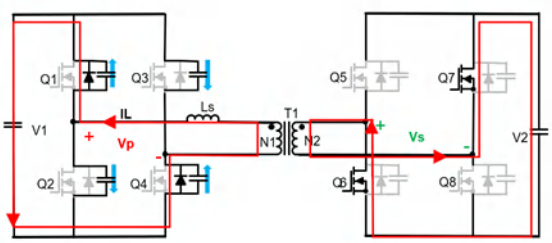

(a) Mode 1 (t0 to t0').

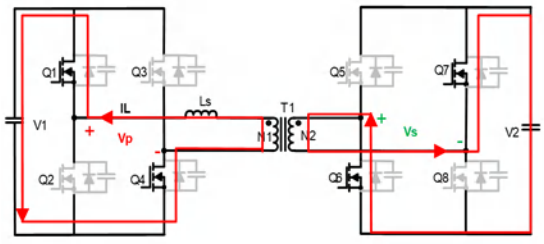

(b) Mode 2 (t0' to t1).

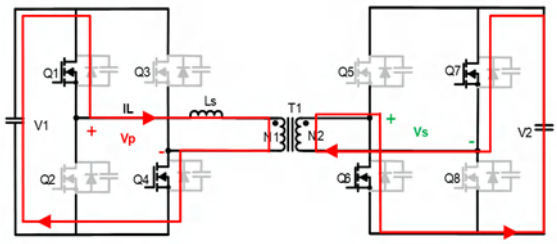

(c) Mode 3 (t1 to t2).

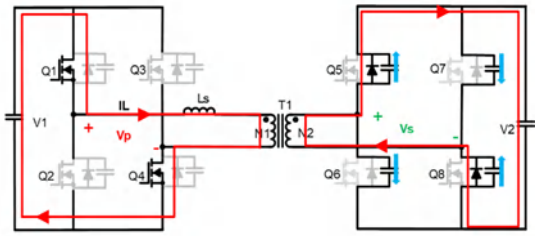

(d) Mode 4 (t2 to t2').

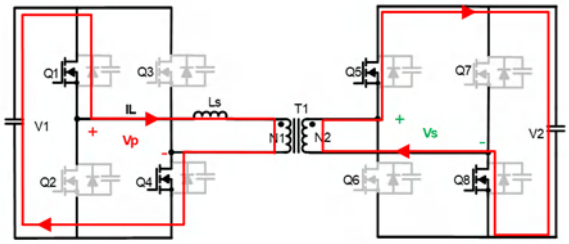

(e) Mode 5 (t2' to t3).

Figure 7. *Operation modes of DAB under SPS control.*

DAB Converter Challenges Under SPS Control

In a DAB converter, SPS control is the easiest control to implement. Conversely, there are some challenges when running this control. At first, all primary switches turn off at the peak point of inductor current as shown in **Figure 8** and this high turn-off current will increase the turn-off losses. Besides, V_p and V_s are both square wave voltages and their interaction is through the inductor L_s, so the phase of the primary current is not always the same as the primary voltage. As **Figure 8** shows, I_L is of the opposite phase from V_p for an interval of t0 to t1 and t2 to t3, that is a portion of the delivered power that is sent back to the primary voltage source V1. We defined it as backflow power, which is the shadow area in **Figure 8**. For a given transmission power, the input power increases to compensate the loss caused by backflow power with the increasing backflow power. Therefore, the circulating power and current are increased, which results in significant losses in power devices and magnetic components.

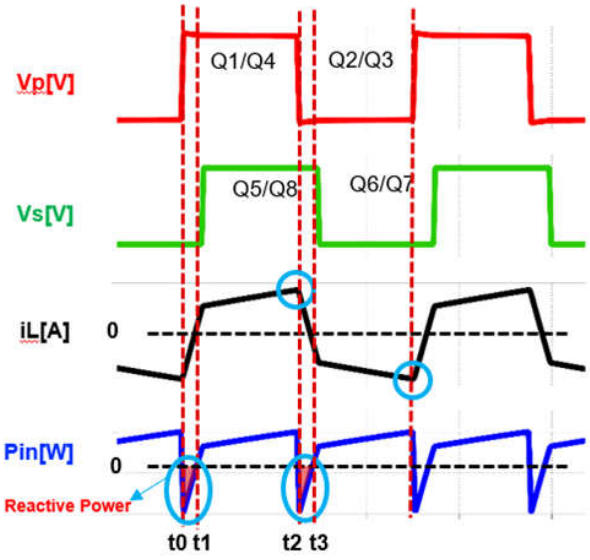

Figure 8. *Turn-off current and reactive power waveforms.*

In addition, the soft switching range of the DAB is also affected by the load. The energy stored in L_S is the key to realize soft switching on both sides. Especially at light load, less energy is stored in L_s, this is insufficient to discharge the FETs' output capacitors for soft switching. **Equation 5** represents the minimum current required by the topology to discharge the capacitors.

$$\frac{I_{Lmin}^2 \times L_s}{2} \gg \frac{V_1^2 \times \left(4 \times C_{oss}\right)}{2} \tag{5}$$

where

- C_{oss} is output parasitic capacitance of Q1

The existing literature [6]–[9] proposes methods to increase the degree of freedom to improve this situation, such as multiple phase shift control, multiple phase shift plus variable duty, or frequency control methods. However, the increase in degree of freedoms also leads to more complex system analysis and control.

Multi-Degree-of-Freedoms (MDOF) Optimization Process

This section introduces how to perform multi-degree-of-freedoms (MDOF) optimization on DAB. MDOF optimization includes four parts, as shown in **Figure 9**. We will introduce each part individually by focusing on the DAB modulation methods, mathematical models, optimization objectives, and optimization algorithm.

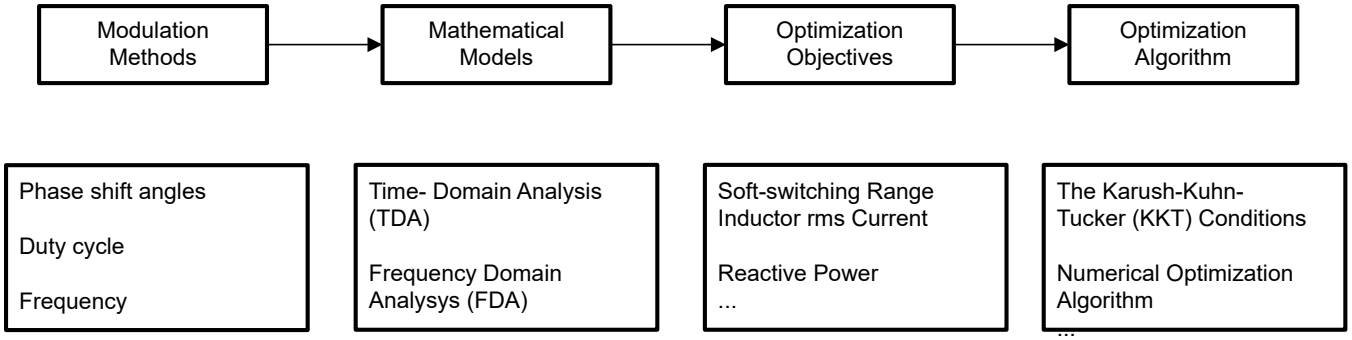

Figure 9. *Multiple degrees-of-freedom optimization process.*

Modulation Methods

The modulation method is the selection of multi-degree-of-freedoms, typically, it is phase shift angle, duty cycle, and frequency. We can use one of these methods or combine them to achieve a more advanced control technique. In this section, we will only introduce the phase shift angles modulation method and explore the relationship between different multiple phase shift modulation methods for a DAB converter. Multiple phase shift modulation usually includes dual phase shift control (DPS), extended phase shift control (EPS), triple phase shift control (TPS). **Figure 10** gives the definition of each phase shift angles and shows the relationship of these modulation methods. The left side waveforms in **Figure 10** are the typical waveforms of a TPS control, based on the waveform, there are a total of three phase shift angles:

- $Ø_a$ is defined as the internal phase shift angle in the primary side (phase shift angle between Q1 and Q4)
- $Ø_b$ is defined as the external phase shift angle between the primary and the secondary side (phase shift angle between Q1 and Q5)
- $Ø_c$ is defined as another internal phase shift angle in the secondary side (phase shift angle between Q5 and Q8)

The middle figure in **Figure 10** shows the relationship between different modulation methods. Observe that SPS, DPS, and EPS are special modes of TPS. Note that when the $Ø_a$ or $Ø_c$ are equal to 0, the control is operating in EPS mode. When $Ø_a$ is equal to $Ø_c$, the converter is running in DPS mode. When Øa and Øc are equal to 0, the DAB is working in SPS mode. The previous chapter showed the waveform under SPS control which the square voltage of bridges is a two-level wave. However, for DPS, EPS, and TPS control, the square voltage of bridges become a three-level wave due to the inner phase shift angle effect as shown in **Figure 10**.

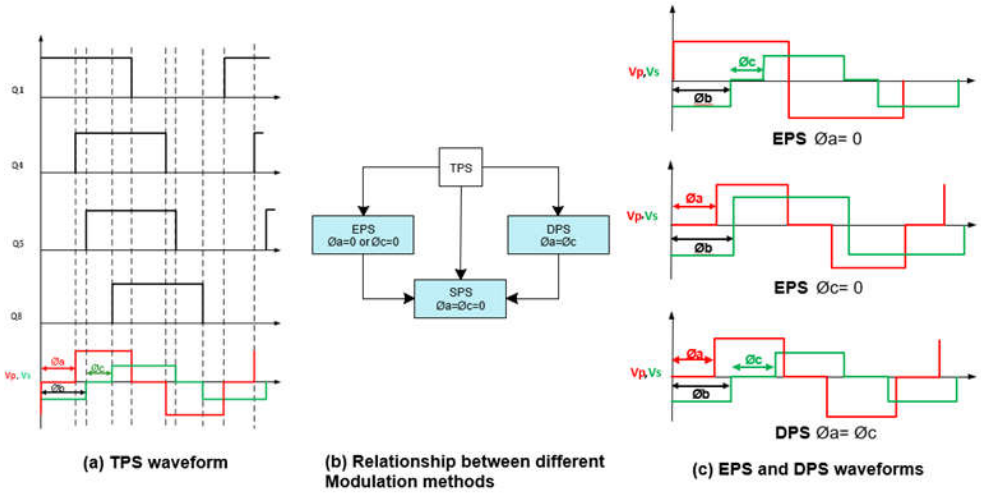

Figure 10. *Multiple phase shift overview.*

Compared to SPS, the maximum transmission power of multiple phase shift angle control is the same as SPS control. However, adding a third level on both the H-Bridge converters helps in decreasing current stress, improving efficiency and expanding the ZVS range. **Figure 11** shows the simulation comparison between DPS and SPS control, by changing the multi-waveform V_p from 2-level to 3-level, the opposite phase between V_p and I_L decrease, which helps reduce the reactive power. In addition, the inner phase shift angle changes the slope of inductor current which helps decrease the current stress of Q4 and Q5. For more detailed analysis related to DPS, EPS, and TPS control see [7]–[13].

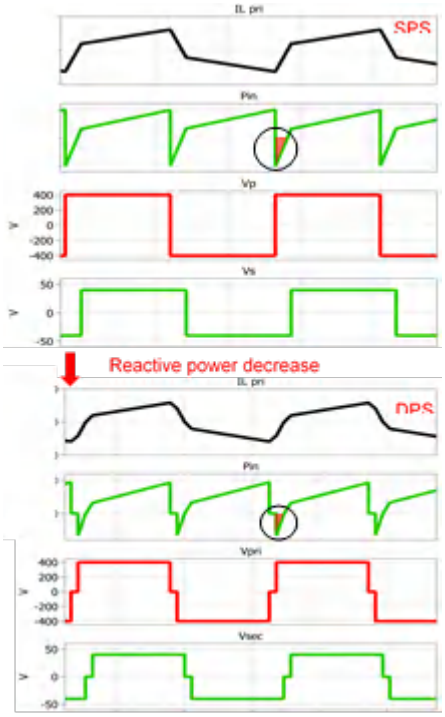

(a) Reactive power comparison.

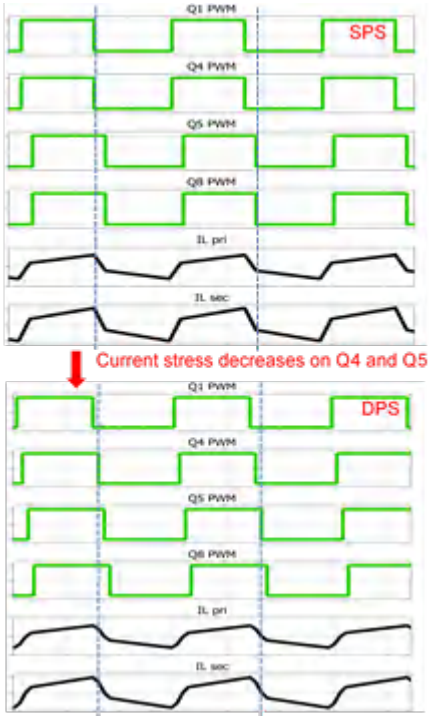

(b) Current stress comparison.

Figure 11. *Comparison waveforms between SPS and DPS.*

Table 2 shows a high-level summary between different control methods. Notice that TPS can achieve the best performance using the highest control complexity. For more detailed comparisons between different modulation methods, see [14]–[15].

	SPS control	EPS and DPS control	TPS control
Number of control freedom	1	2	3
Reactive power	high	medium	low
RMS current	high	medium	low
Soft-switching range	narrow	Wider than SPS	Wider than EPS/DPS
Control complexity	low	medium	high
Total efficiency	low	medium	high

Table 2. *Different phase shift modulation methods comparison.*

Mathematical Models

As described in **Modulation Methods**, when adopting multiple phase shift control, there are multiple operation modes due to the different combinations of phase shift angles. For example, there are a total of six operation modes for TPS control when there is unidirectional operation as mentioned in [16]. The transferred power, reactive power, and current stress are different under different modes. Therefore, to describe these features based on quantitative analysis under different modes, we need to build mathematical models based on different modes. The complexity of the model also determines the construction of objectives and the choice of algorithms. The general mathematical models are based on Time-Domain Analysis (TDA) and Frequency-Domain Analysis (FDA). We will use one of the TPS operation mode to briefly explain these mathematical models.

TDA Model Analysis

For TDA models, deducing the voltage and current expression during different time intervals is necessary. **Figure 12** is one of the TPS operation modes and **Figure 13** is a simplified model of the DAB, which actually shows two square waves (V_p and V_s) across the inductor. Therefore, the inductor voltage and current equation across the inductor can be written as:

$$V_L(t) = V_p - N \times V_s \tag{6}$$

$$I_L(t_x) = I_L(t_{x-1}) + \frac{1}{L_s} \times \int_{t_{x-1}}^{t_x} V_L(t) \times dt \tag{7}$$

where

- t_{x-1} denotes the initial moment of the working mode
- t_x denotes the final moment of the working mode

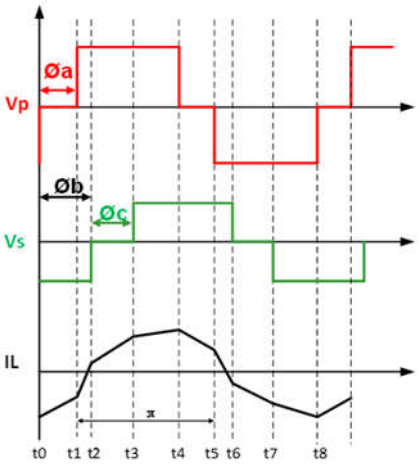

Figure 12. *Operation waveforms under TPS.*

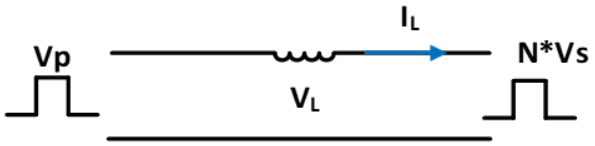

Figure 13. *Simplified DAB model.*

At the same time, we can also calculate the expression for the effective value of the series inductor current as:

$$I_{L_{rms}}(t) = \sqrt{\frac{\int_{t0}^{t0+T_s} I_L^2(t) \times dt}{T_s}} \tag{8}$$

After having the expressions of current and voltage, we can easily calculate the expression for instant power. Additionally, by performing integration, we can get the expression of average power in **Equation 9** and **Equation 10**. Based on these equations, we can obtain the magnitude of the transmission power in different modes, as well as the expressions for the corresponding node currents.

$$P_1(t) = \frac{\sqrt{\int_{t0}^{t0+T_s} V_p \times I_L(t) \times dt}}{T_s} \tag{9}$$

$$P_2(t) = \frac{\sqrt{\int_{t0}^{t0+T_s} N \times V_s \times I_L(t) \times dt}}{T_s} \tag{10}$$

FDA Model Analysis

Another mathematical analysis method is FDA. For better analysis, we redefine phase shift angles like **Figure 14** and this could simplify the math process. The blue waves in **Figure 14** are the equivalent components of V_p and V_s, which means the fundamental component. Based on the V_p and V_s square waves, we can write the expression of its fundamental wave as shown **Equation 11** in and **Equation 12**, thus we can easily derive the expression for the current.

$$V_{p\_FDA}(t) = \frac{4 \times V_p \times \cos\alpha \times \sin(\omega \times t)}{\pi} \tag{11}$$

$$V_{s\_FDA}(t) = \frac{4 \times N \times V_s \times \cos\gamma \times \sin(\omega \times t - \beta)}{\pi} \tag{12}$$

Note that the above expressions only consider the fundamental component; some FDA analysis also consider higher harmonics, which can increase the accuracy of the analysis but will greatly increase the complexity.

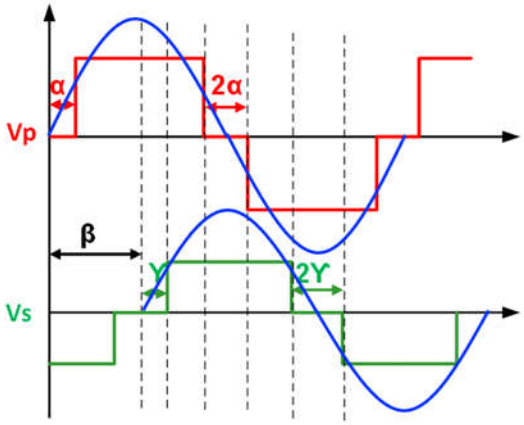

Figure 14. *Operation waveforms under TPS.*

Previously, we provided a brief introduction to the mathematical methods used when analyzing the converter. **Table 3** summarizes these mathematical modeling methods. Generally, TDA has the highest complexity because it produces more operating intervals and operating modes, while FDA only considers the fundamental wave is simplest. For the accuracy, both TDA and FDA considering higher harmonics have high accuracy, while FDA that only considers the fundamental wave has the lowest. The generality of FDA methods is usually good, which means it is more flexible to use this method to analyze other DAB structures without considering each time interval, overlap range, or working mode. In contrast, TDA is difficult to expand directly to other structures. The working mode and expression derivation need to be modified if the topology is changed.

Mathematical models		Complexity	Generality	Accuracy
TDA		High	Low	High
FDA	Fundamental component only	Low	Medium	Low
	Consider multiple harmonics	Medium	High	Medium

Table 3. *Different mathematical model comparison.*

Considerations of Optimization Objectives

After building mathematical models, we need to choose optimization objectives. To optimize the efficiency of the DAB converter, it is important to understand the different types of losses that contribute to the overall loss. The losses in the DAB can be classified into two main categories: power switch device losses and magnetic device losses. **Figure 15** shows the main loss distribution of a DAB converter. The power switch device losses include switching losses and conduction losses, while magnetic device losses include copper losses and core losses, as shown in **Figure 15**. Switching losses include the turn on losses and turn off losses. Turn on loss depends on whether the switches can achieve ZVS. However, ZVS range has a boundary under different conditions [17]. Turn off loss is related to current value when switches are turned off. Both conduction loss and copper loss are directly affected by the inductor RMS current. Core loss is mainly depending on the operating frequency, magnetic flux density as well as core material and this loss tends to be a uniform loss that does not vary significantly with power when operating conditions are specified. Therefore, the optimization objectives can be divided into ZVS range, turn-off current, effective value of inductor current. Optimizing all of these objectives will greatly increase the complexity of building the mathematical model. Therefore, we usually choose one or two main objectives, such as ZVS range, inductor current stress or reactive power as the optimization path in practical applications.

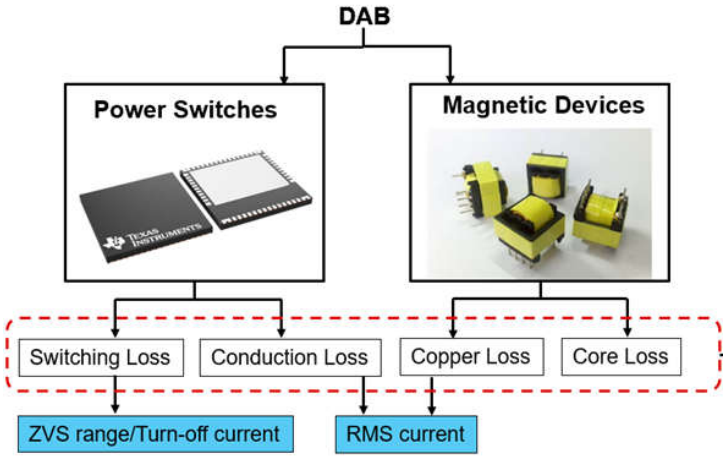

Figure 15. *Loss distribution of DAB.*

Selection of Optimization Algorithms

Selecting the optimization algorithm to better match the objectives is the final step of the MDOF optimization process. In the case of multi-degree of freedoms control, there is often strong coupling between various degrees of freedom, so some algorithm methods are proposed to help calculate the optimal solution. This paper does not describe those methods but more details are in the reference [18].

Series Resonant DAB (SR-DAB) Overview and the Control Method

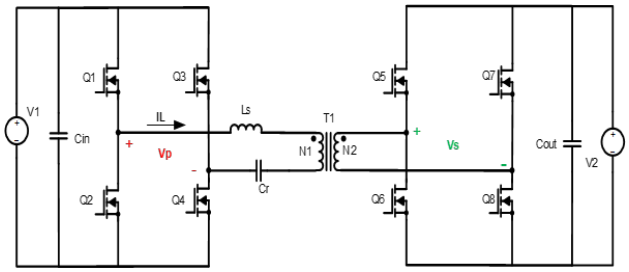

Figure 16. *Schematic representation of an SR-DAB converter.*

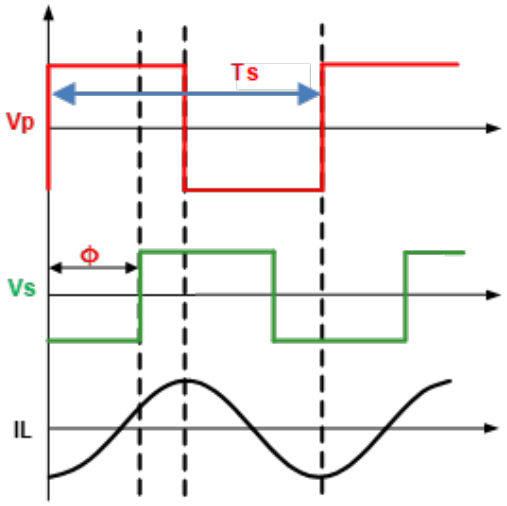

Figure 17. *Waveforms of SR-DAB converter.*

By inserting a series resonant tank in the DAB converter, it forms the SR-DAB as shown in **Figure 16**. The resonant tank can be placed in primary or secondary side. And the resonant capacitor can also be split in both sides [19]. Placement of capacitances in primary and secondary prevents dc injection from both the active bridges thus avoiding transformer saturation. However, it will increase the total system cost.

As depicted in **Figure 16**, switches Q1 –Q4 form the primary side full bridge and they are modulated to generate V_p. The secondary side full bridge of the converter consists of Q5 –Q8, which are modulated to generate a voltage V_s. As mention in **Single-Phase-Shift (SPS) DAB Operation Principles**, the external phase shift Ø between V_p and V_s

determines the direction of the power flow, with positive Ø meaning the forward operation which corresponds to the case where V_p leads V_s.

Figure 17 shows the basic operation waveform under SPS control. Similar as the series resonant converter, the SR-DAB converter needs to operate at frequency higher than resonant frequency to make sure the converter operates in the inductive region. Due to the resonance features of the circuit, the inductor current of SR-DAB is almost sinusoidal, which will lead to a smaller turn-off current and rms current compared to a traditional DAB. Since the fundamental components of the resonant tank current and bridge voltages are the main sources of the power transfer, the FDA method can be used to build its mathematical models. By using the First Harmonic Analysis (FHA), the normalized average transition power P_o is expressed in **Equation 13**. Find more details in the reference [4].

$$P_o = \frac{8 \times M \times \sin\emptyset}{\pi^2 \times Q \times \left(F - \frac{1}{F}\right)} \left(-\pi \le \emptyset \le \pi \right) \tag{13}$$

where

$$M = \frac{N_1 \times V_2}{N_2 \times V_1} F = \frac{f_s}{f_r} f_r = \frac{1}{2 \times \pi \times \sqrt{L_s \times C_r}} f_s = \frac{1}{T_s} Q = \frac{\sqrt{L_s / C_r}}{R} R = \frac{V_2}{I_o}$$

Similar to the traditional DAB converter, the multiple degree of freedom control method is also available for SR-DAB converter. **Table 4** summarizes the common used control methods in SR-DAB. It is concluded that better performance is achieved when the numbers of controlled variables is increased. TPS control with a fixed frequency can achieve better performance compared to the SPS control. Conversely, it cannot achieve full load range soft-switching except the light load condition. By introducing the switching frequency as another control freedom, frequency is used to control the power transfer amount, while the phase shift angles can be used as constraint conditions to optimize the current stress, soft-switching range, and reactive power [20].

	SPS + fix frequency	SPS + variable frequency	TPS + fix frequency	TPS + variable frequency
Numbers of freedom degree	1	2	3	4
Soft-switching	Not below half load	Not at light load	Not at light load	Yes
RMS current	high	medium	low	low
Control complexity	low	medium	high	high
Total efficiency	low	medium	high	highest

Table 4. *Different SR-DAB control methods comparison.*

Figure 18 shows the simulation results which compare the TPS control DAB and TPS control SR-DAB when having a variable frequency. It is obvious to see the SR-DAB has lower peak current, which decreases 11% compared to DAB. As a consequence, the turn off loss is decreased, thus improving the system efficiency and decreasing the current stress in switching devices.

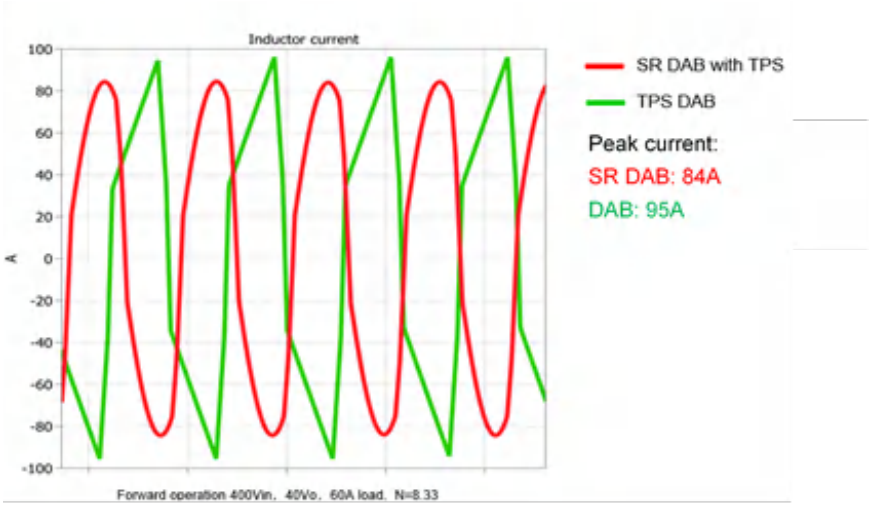

Figure 18. *Simulation waveforms of DAB and SR-DAB.*

DAB Design Example

SR-DAB Design Features

To demonstrate the theory explained thus far, a 3.6kW SR-DAB reference design [21] targeting ESS applications with battery voltage ranging from 40VDC to 60VDC is used as a reference. **Figure 19** and **Figure 20** show the block diagram and board photo of this reference design, respectively. The reference design uses the TMS320F28P55 C2000™ microcontroller to control the SR-DAB on both sides, and silicon carbide FETs for high input voltage applications (550VDC maximum). The resonant capacitors are split to both sides which will help to block the DC components. The total power-stage dimensions are 250mm × 130mm × 50mm. The peak efficiency of this design is 98.5%.

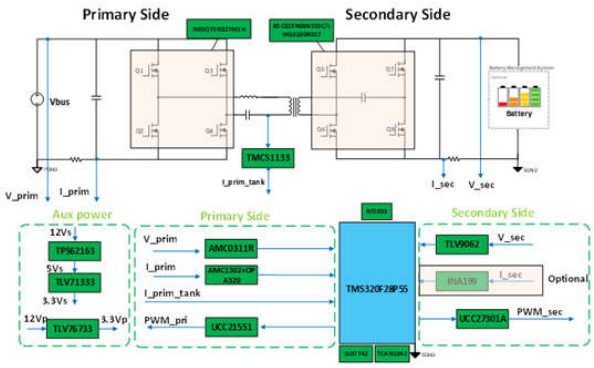

Figure 19. *3.6kW SR-DAB reference design block diagram.*

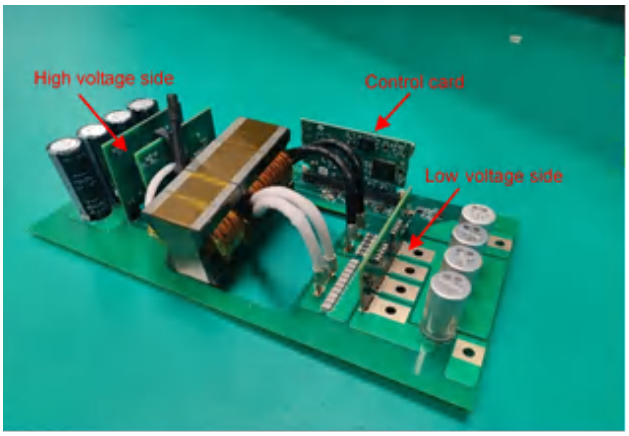

Figure 20. *3.6kW SR-DAB reference design.*

SR-DAB Design Process

This chapter introduces how to use MDOF optimization process discussed in **Multi-Degree-of-Freedoms (MDOF) Optimization Process** to design an SR-DAB converter. As we already compared the performance of different SR-DAB control methods, we choose the TPS + variable frequency as the modulation method to achieve the best performance. We decouple frequency from the phase shift angle, using frequency to control power and using the phase shift angle to optimize the performance. For the design with multiple degrees of freedom, we need to choose the optimization

targets. Because this design is targeting the ESS applications, the current is high in the low-voltage side with the power increasing. In this phenomenon, there will be higher turn off loss if the turn off current in the low-voltage side is high. Therefore, the targets we hope to optimize in this design is turn-off current in the low-voltage side and the reactive power. After confirming the optimization targets, by performing the FDA, we can obtain the expressions of Vp and Vs after normalization:

$$V_{p\_pu}(t) = \frac{4 \times \cos(\emptyset_a) \times \sin(\omega \times t)}{\pi} \tag{14}$$

$$V_{s\_pu}(t) = \frac{4 \times M \times \sin(\omega \times t - \emptyset_b)}{\pi} \tag{15}$$

Because the converter is operating higher than the resonant frequency to make the resonant tank located in the inductive region, the resonant voltage Vres is 90° ahead of the current IL. In addition, based on the constraints, achieving the minimum turn-off current on the low-voltage side, that is IL ($\emptyset_b$) = 0. **Equation 16** and **Equation 17** show the constraint equations.

$$\frac{V_{res_{pu}}\left(\emptyset_b + \frac{\pi}{2}\right)}{Zr} = IL(\emptyset_b) = 0 \tag{16}$$

$$V_{res_{pu}}\left(\emptyset_b + \frac{\pi}{2}\right) = V_{p\_pu}\left(\frac{\pi}{2} + \emptyset_b\right) - V_{s_{pu}}\left(\frac{\pi}{2} + \emptyset_b\right) = 0 \tag{17}$$

where

- Zr is the impedance of the resonant tank

Based on **Figure 21** and to realize the zero reactive power, we only need to make $\emptyset_a = \emptyset_b$. According to these constraint equations, the corresponding phase shift angles can be calculated using **Equation 18** and **Equation 19**:

$$\cos(\emptyset_a) \times \cos(\emptyset_b) = M \tag{18}$$

$$\emptyset_a = \emptyset_b \tag{19}$$

The simulation waveforms in **Figure 21** show the result that uses the proposed optimization methods. As shown in the figure, reactive power is eliminated and the low-voltage side is turned off when the current is 0, which greatly optimizes the conduction loss and switching loss. **Figure 22** shows the experimental test waveforms under steady state with bidirectional operation.

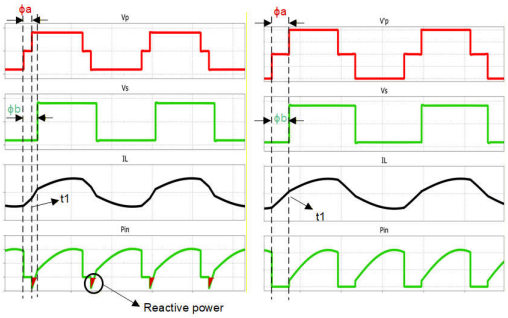

Figure 21. *Simulation waveforms based on proposed method.*

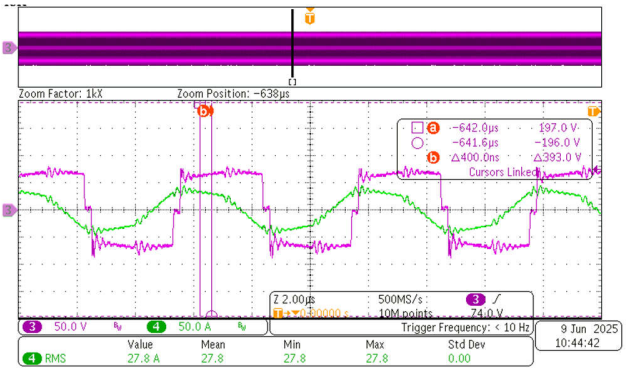

(a) Vin = 400V, Vo = 60V: Forward operation.

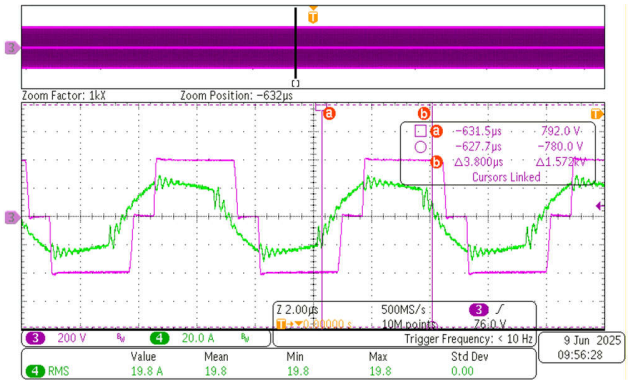

(b) Vin = 40V, Vo = 400V: Reverse operation.

Figure 22. *Experimental waveforms.*

Conclusions

This paper describes DAB fundamentals including operational principles, design challenges under SPS control, multiple degree of freedoms optimization processes, and SR-DAB overview and its control method. We have observed that DAB is a good candidate for applications that require a wide input/output voltage range. Conversely, we observed that SR-DAB is a better candidate because switching current and RMS can significantly decrease. This allows an increase in the efficiency and a reduction in the EMI with respect to the DAB converter. A design of SR-DAB is built to verify the performance under wide gain range applications.

References

1. Federal Consortium for Advanced Batteries, "Executive Summary - National Blueprint for Lithium Batteries 2021-2030"
2. H. Huang, "Designing an LLC resonant half-bridge power converter," Texas Instruments Power Supply Design Seminar SEM1900, 2010-2011.
3. S. Yu, X. Gong, G. Wang, M. Bhardwaj, "Designing a High-Power Bidirectional AC/DC Power Supply Using SiC FETs," Texas Instruments Power Supply Design Seminar SEM2400, 2020-2021.
4. X. Li and A. K. S. Bhat, "Analysis and Design of High-Frequency Isolated Dual-Bridge Series Resonant DC/DC Converter," in IEEE Transactions on Power Electronics, vol. 25, no. 4, pp. 850-862, April 2010
5. F. Khan, S. S. Nag and B. Singh, "Analysis, Design, and Comparison of Isolated DC-DC Converters for Traction Application," 2023 IEEE Transportation Electrification Conference & Expo (ITEC), Detroit, MI, USA, 2023, pp. 1-6
6. N. Noroozi, A. Emadi and M. Narimani, "Performance Evaluation of Modulation Techniques in Single-Phase Dual Active Bridge Converters," in IEEE Open Journal of the Industrial Electronics Society, vol. 2, pp. 410-427, 2021
7. D. C. Pandey, P. K. Behera and M. Pattnaik, "Steady-State Analysis of Dual Active Bridge Converter with Single Phase Shift and Dual Phase Shift Modulation," 2023 IEEE International Students' Conference on Electrical, Electronics and Computer Science (SCEECS), Bhopal, India, 2023, pp. 1-6
8. H. Wen and W. Xiao, "Bidirectional dual-active-bridge DC-DC converter with triple-phase-shift control," 2013 Twenty-Eighth Annual IEEE Applied Power Electronics Conference and Exposition (APEC), Long Beach, CA, USA, 2013

9. Zhao, Q. Yu and W. Sun, "Extended-Phase-Shift Control of Isolated Bidirectional DC–DC Converter for Power Distribution in Microgrid," in IEEE Transactions on Power Electronics, vol. 27, no. 11, pp. 4667-4680, Nov. 2012
10. H. Shi et al., "Minimum-Backflow-Power Scheme of DAB-Based Solid-State Transformer with Extended-Phase-Shift Control," in IEEE Transactions on Industry Applications, vol. 54, no. 4, pp. 3483-3496
11. S. Chaurasiya and B. Singh, "A Load Adaptive Hybrid DPS Control for DAB to Secure Minimum Current Stress and Full ZVS Operation Over Wide Load and Voltage Conversion Ratio," in IEEE Transactions on Industry Applications, vol. 59, no. 2, pp. 1901-1911, March-April 2023
12. C. Pandey, P. K. Behera and M. Pattnaik, "Steady-State Analysis of Dual Active Bridge Converter with Single Phase Shift and Dual Phase Shift Modulation," 2023 IEEE International Students' Conference on Electrical, Electronics and Computer Science (SCEECS), Bhopal, India, 2023, pp. 1-6
13. Q. Zeng, Y. Wei, B. Yang, J. Xu and D. Zhao, "Research on DAB Triple Phase Shift Control Strategy Based on Current Stress and Soft Switch Dual Objective Optimization," 2021 11th International Conference on Power and Energy Systems (ICPES), Shanghai, China, 2021, pp. 36-41
14. F. Corti, V. Bertolini, A. Reatti, E. Cardelli and M. Giallongo, "Comparison of Control Strategies for Dual Active Bridge Converter," 2022 IEEE 21st Mediterranean Electrotechnical Conference (MELECON), Palermo, Italy, 2022, pp. 902-907
15. Kumar, A. H. Bhat and P. Agarwal, "Comparative analysis of dual active bridge isolated DC to DC converter with double phase shift and triple phase shift control techniques," 2017 Recent Developments in Control, Automation & Power Engineering (RDCAPE), Noida, India, 2017, pp. 257-262
16. Y. A. Harrye, K. H. Ahmed, G. P. Adam and A. A. Aboushady, "Comprehensive steady state analysis of bidirectional dual active bridge DC/DC converter using triple phase shift control," 2014 IEEE 23rd International Symposium on Industrial Electronics (ISIE), Istanbul, Turkey, 2014, pp. 437-442
17. P. He and A. Khaligh, "Comprehensive Analyses and Comparison of 1 kW Isolated DC–DC Converters for Bidirectional EV Charging Systems," in IEEE Transactions on Transportation Electrification, vol. 3, no. 1, pp. 147-156, March 2017
18. D. Mou et al., "Optimal Asymmetric Duty Modulation to Minimize Inductor Peak-to-Peak Current for Dual Active Bridge DC–DC Converter," in IEEE Transactions on Power Electronics, vol. 36, no. 4, pp. 4572-4584, April 2021
19. U. Kundu, B. Pant, S. Sikder, A. Kumar and P. Sensarma, "Frequency Domain Analysis and Optimal Design of Isolated Bidirectional Series Resonant Converter," in IEEE Transactions on Industry Applications, vol. 54, no. 1, pp. 356-366, Jan.-Feb. 2018
20. M. Yaqoob, K. H. Loo and Y. M. Lai, "A Four-Degrees-of-Freedom Modulation Strategy for Dual-Active-Bridge Series-Resonant Converter Designed for Total Loss Minimization," in IEEE Transactions on Power Electronics, vol. 34, no. 2, pp. 1065-1081, Feb. 2019
21. 3.6kW bidirectional SR-DAB converter reference design for energy storage system: **PMP41134 reference design | TI.com**

IMPORTANT NOTICE AND DISCLAIMER

TI PROVIDES TECHNICAL AND RELIABILITY DATA (INCLUDING DATASHEETS), DESIGN RESOURCES (INCLUDING REFERENCE DESIGNS), APPLICATION OR OTHER DESIGN ADVICE, WEB TOOLS, SAFETY INFORMATION, AND OTHER RESOURCES “AS IS” AND WITH ALL FAULTS, AND DISCLAIMS ALL WARRANTIES, EXPRESS AND IMPLIED, INCLUDING WITHOUT LIMITATION ANY IMPLIED WARRANTIES OF MERCHANTABILITY, FITNESS FOR A PARTICULAR PURPOSE OR NON-INFRINGEMENT OF THIRD PARTY INTELLECTUAL PROPERTY RIGHTS.

These resources are intended for skilled developers designing with TI products. You are solely responsible for (1) selecting the appropriate TI products for your application, (2) designing, validating and testing your application, and (3) ensuring your application meets applicable standards, and any other safety, security, regulatory or other requirements.

These resources are subject to change without notice. TI grants you permission to use these resources only for development of an application that uses the TI products described in the resource. Other reproduction and display of these resources is prohibited. No license is granted to any other TI intellectual property right or to any third party intellectual property right. TI disclaims responsibility for, and you fully indemnify TI and its representatives against any claims, damages, costs, losses, and liabilities arising out of your use of these resources.

TI’s products are provided subject to TI’s Terms of Sale, TI’s General Quality Guidelines, or other applicable terms available either on ti.com or provided in conjunction with such TI products. TI’s provision of these resources does not expand or otherwise alter TI’s applicable warranties or warranty disclaimers for TI products. Unless TI explicitly designates a product as custom or customer-specified, TI products are standard, catalog, general purpose devices.

TI objects to and rejects any additional or different terms you may propose.

Last updated 10/2025